Supporting Information

Tailorable polarity-flipping response in self-powered, flexible Sb_2Se_3/ZnO bilayer photodetectors

Jinchun Jiang, [†a] Yujie Guo, [†a] Xiaoliang Weng,[a] Fangchao Long,[a] Yun Xin,[ab] Yangfan Lu,[b] Zhizhen Ye,[b] Shuangchen Ruan,[a] Yu-Jia Zeng[*a]

[a.] *Key laboratory of Optoelectronic Devices and Systems of Ministry of Education and Guangdong Province, College of Physics and Optoelectronic Engineering, Shenzhen University, Shenzhen, 518060, P. R. China.*
[b.] *State Key Laboratory of Silicon Materials, School of Materials Science and Engineering, Zhejiang University, 310027, P. R. China.*
† Jinchun Jiang and Yujie Guo contributed equally to this paper.

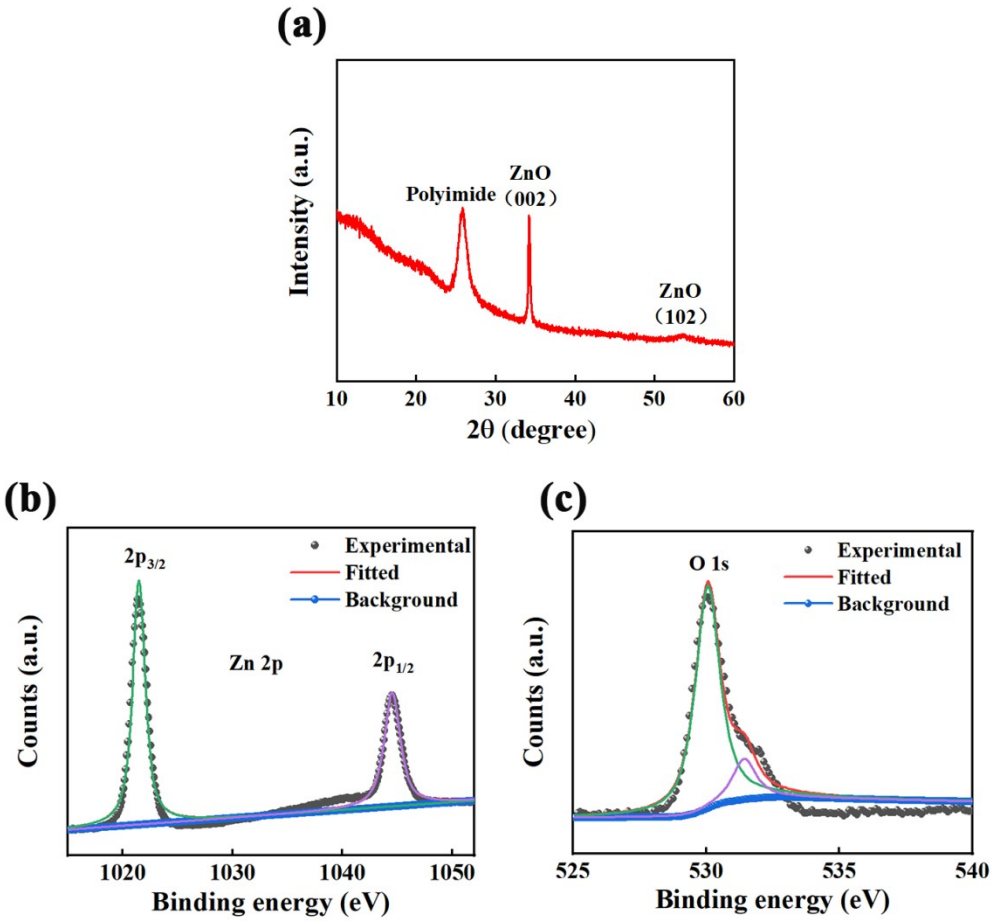

Fig. S1. (a) XRD pattern of ZnO thin film grown on the polyimide substrate. XPS spectra of ZnO thin film of (b) Zn 2p; and (c) O 1s core levels

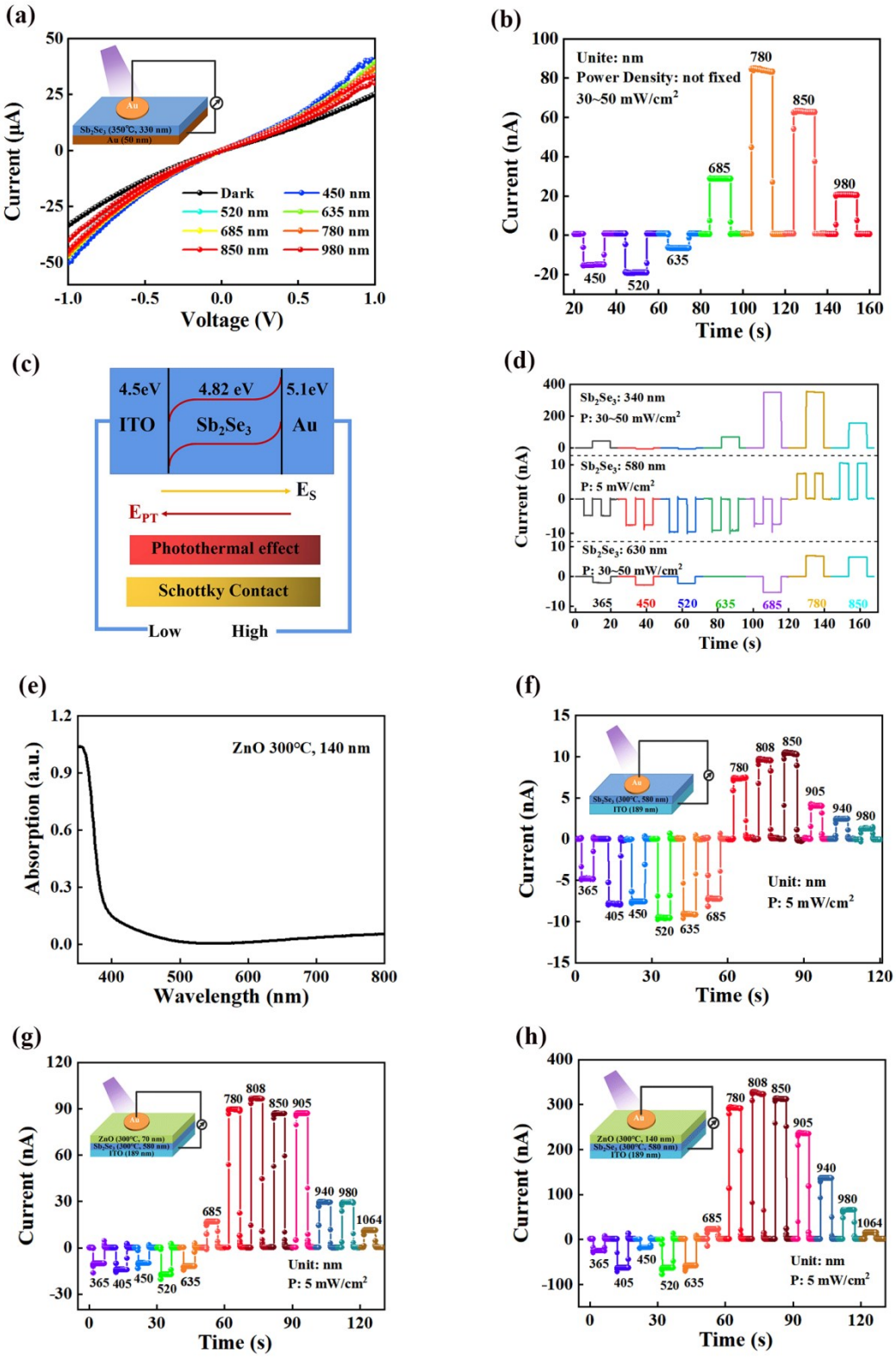

Fig. S2. (a) I-V curves of the ITO/Sb_2Se_3/Au device in the dark and under different light illuminations with a power density of 5 mW/cm^2. The inset shows scheme of the PD. b) Time-resolved photoresponse of the ITO/Sb_2Se_3/Au device under different light illuminations at zero bias. (c) Schematics of band alignment and working mechanism of the ITO/Sb_2Se_3/Au device PDs under light illumination. (d) I-t curves of the ITO/Sb_2Se_3/Au PD under selective light illumination with different Sb_2Se_3 thickness. (e) Absorption spectrum of ZnO. (f)-(h) I-t curves of the ITO/Sb_2Se_3/ZnO/Au device under different light illuminations with different ZnO thickness. (f) ZnO: 0 nm. (g) ZnO: 70 nm. (h) ZnO: 140 nm. The insets show the corresponding device configuration.

The Sb_2Se_3 layer should be grown in a thickness range, such that a temperature gradient can be created to establish the internal potential for dual-polarity behavior. As shown by the I-t curves in Figure S2a, Sb_2Se_3 layers with thickness of 340 nm, 580 nm and 630 nm reveals huge divergence in photoresponse. To start with, a red-shift of the flipping wavelength (635 nm-780 nm) is witnessed as the layer thickens. This result verifies the inverse correlation between the incident wavelengths and their absorption depth in Sb_2Se_3, as reported before. To test the penetration depth under 365 nm exposure, we used a 365 nm continuous wave laser (136.7 mW) of substantially higher intensity than the visible-NIR lasers (5.75 -12.02 mW). As demonstrated in the topmost I-t curve, the photocurrent reverses its direction when the incident wavelength decreases from the visible to UV region. This indicates the vanishment of PTE effect upon strong UV radiance. Thus, UV photons are able to travel across the whole Sb_2Se_3 layer to reach the bottom ITO electrode. We therefore deduce that the thickness of 340 nm is too thin to meet our experimental requirements. On the flip slide, both 580 nm and 630 nm are thickness enough to sustain a temperature gradient in the direction perpendicular to the layer surface.

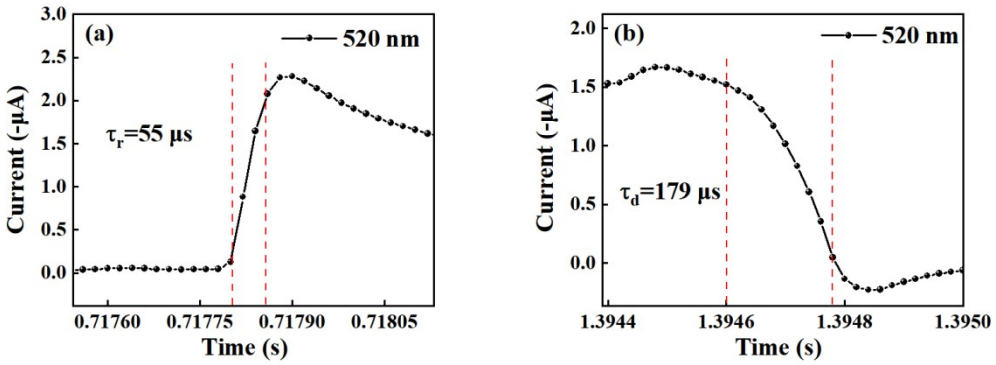

Fig. S3. (a) Rise time (τ_r) and (b) decay time (τ_d) under 520 nm illumination. The PD was stacked by the 300 ℃ sputtered Sb_2Se_3 layer of 580 nm and 300 ℃ sputtered ZnO layer of 140 nm.

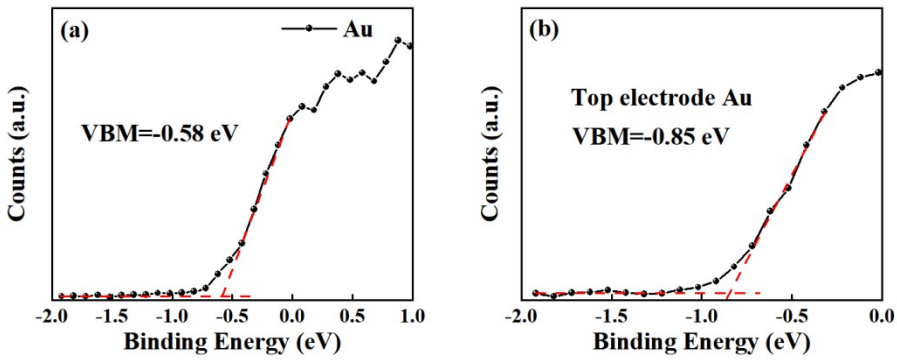

Fig. S4. (a) Binding energy of Au on the Si/SiO_2 substrate. (b) Binding energy of the top electrode Au.

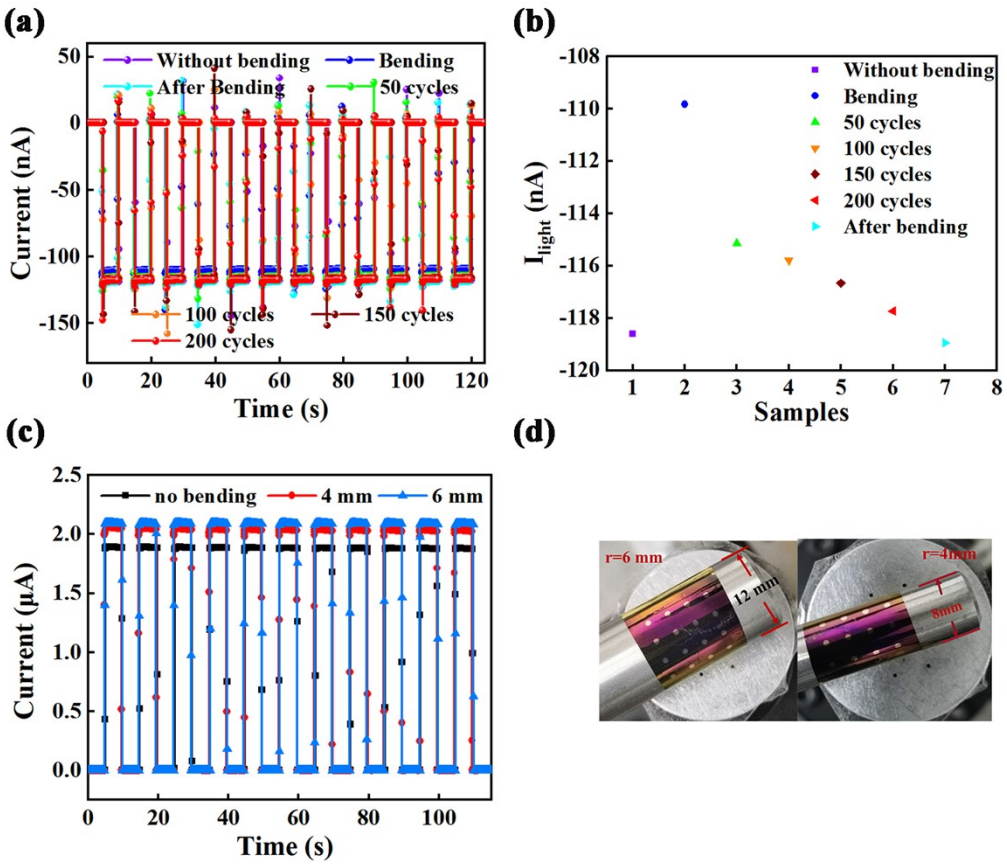

Fig. S5. (a) Time-resolved response of the flexible Au/Sb_2Se_3/ZnO/Au PD under the 520 nm illumination, which were measured under the conditions of no bending, under bending (50, 150, 200 cycles) and after bending. (b) Values of the corresponding photocurrent. (c) I-t curves of the flexible PD under the 905 nm illumination and tensile strain, whose bending radius are 4mm and 6mm, respectively. (d) The image of the devices.

Table S1 The properties of the optimized Sb_2Se_3/ZnO PD under zero bias with different wavelengths.

Wavelength (nm)	Iph (A)	Ion/Ioff	R (mA/W)	D* (Jones)
365	-6.84×10^{-8}	25	-2.74	-6.60×10^{9}
405	-4.45×10^{-7}	203	-17.80	-4.76×10^{10}
450	-3.37×10^{-7}	173	-13.50	-3.83×10^{10}
520	-4.71×10^{-7}	248	-18.86	-5.43×10^{10}
635	-2.76×10^{-7}	119	-11.03	-2.88×10^{10}
685	-8.91×10^{-8}	38	-3.56	-9.32×10^{9}
780	4.37×10^{-7}	281	17.48	5.53×10^{10}
808	6.35×10^{-7}	291	25.40	6.78×10^{10}
850	1.29×10^{-6}	655	51.52	1.45×10^{11}
905	1.94×10^{-6}	1238	77.66	2.45×10^{11}
940	1.26×10^{-6}	597	50.55	1.37×10^{11}
980	1.04×10^{-6}	554	41.56	1.20×10^{11}
1064	2.00×10^{-7}	104	8.01	2.27×10^{10}